RAPID COMMUNICATIONS

PHYSICAL REVIEW B VOLUME 46, NUMBER 23 15 DECEMBER 1992-I

Anisotropy of the confined hole states in a (311)*A* AlAs/GaAs/AlAs quantum-well system: Evidence for a camel's-back band structure

R. K. Hayden, E. C. Valadares, M. Henini, and L. Eaves
Department of Physics, University of Nottingham, Nottingham NG7 2RD, United Kingdom

D. K. Maude and J. C. Portal
Service National des Champs Intenses, Centre National de la Recherche Scientifique, Boîte Postale 166X, 38042 Grenoble, France
and Laboratoire de Physique des Solides, Institut National des Sciences Appliquées, 31077 Toulouse, France
(Received 19 May 1992; revised manuscript received 24 August 1992)

Magnetic fields applied parallel to the layer interfaces are used to examine the in-plane energy-band dispersion and anisotropy of the quantum-well states of a double-barrier AlAs/GaAs/AlAs resonant-tunneling diode grown on a (311)*A*-oriented substrate. The measurements reveal biaxial anisotropy in several of the subbands, some of which have a "camel's-back"-shaped structure. These features are confirmed by a six-component envelope-function calculation of the subbands of a (311) valence-band quantum well.

The optical and electronic properties of quantum wells are of fundamental interest since the confinement of the carriers (electrons and holes) leads to behavior that is significantly different from that of bulk semiconductors. Recently, attention has focused on the growth and properties of quantum wells and heterostructures on high-index crystalline planes. In III-V compound heterostructures, such as the GaAs/AlAs system, it has been found that quantum-well lasers grown on the (111)*B* surface have much lower laser threshold currents than similar devices grown on conventional (100) surfaces.[1] Optical measurements have revealed differences in exciton energy[2] and confinement energy[3] between the (100) and higher index planes. Calculations (for example, Refs. 4 and 5) have shown that the electronic structure of valence-band quantum-well states is strongly dependent on substrate orientation. Mobility enhancement of the quasi-two-dimensional hole gas has been observed in modulation doped *p*-type GaAs/(Al,Ga)As heterostructures grown by molecular-beam epitaxy on the (311)*A* GaAs surface using silicon as an acceptor.[6,7] Recently, Santos *et al.* have reported evidence for a weakly pinned hole Wigner crystal in a (311)*A* heterostructure of this type.[8]

In this paper we investigate the form of the energy versus in-plane wave-vector dispersion curves, $\epsilon(\mathbf{k}_{\parallel})$, of the bound hole states in a (311)*A* quantum well based on AlAs/GaAs. The measurements reveal a much greater anisotropy for some of the hole subbands than is observed for those of a similar (100) quantum well.[9] In particular, we find that some of the higher-energy subbands exhibit a pronounced "camel's-back" structure with a saddle point at $k_{\parallel}=0$ and two minima of the hole energy at $k_{\parallel}\simeq(\pm\pi\times10^{6}\ \mathrm{cm}^{-1})$ along the $[01\bar{1}]$ axis of the plane. However, the ground-state subband is found to be isotropic for $k_{\parallel}<1\times10^{6}\ \mathrm{cm}^{-1}$. We compare these results with a six-component envelope-function calculation[10,11] for the (311)*A* valence-band quantum well. It is well known from theoretical considerations that the dispersion curves of the confined holes are quite complicated[12–14] due to the presence of a second-order spin-orbit term in the effective Hamiltonian.[15] This term admixes the light-hole and heavy-hole valence bands and can lead, over certain regions of k space, to the hole energy *decreasing* with *increasing* in-plane wave vector $k_{\parallel}$. In this case, the holes are said to have negative effective mass, or electronlike dispersion. We have recently developed an experimental technique, namely, resonant magnetotunneling spectroscopy,[16] to probe directly the form of the dispersion curves of holes in quantum wells. This technique allows both the magnitude and direction of $\mathbf{k}_{\parallel}$ to be selected, so it can also be used to examine the anisotropy of the carrier dispersion curves with respect to the crystalline axes,[17] including those in strained-layer quantum wells.[18,19]

Figure 1 shows the band diagram and composition of the device under an applied bias V. Details of the growth and composition of this device have been given elsewhere.[20] The inset to the figure shows the orientation of the (311) plane and its principal axes with respect to the conventional cubic unit cell. Holes tunnel into the quantum well with an enregy eV_e from a quasi-two-dimensional hole gas in the emitter accumulation layer. This energy is significantly less than eV, due to the voltage drop across the lightly doped spacer and depletion regions adjacent to the collector barrier.[21] Resonant tunneling from the emitter accumulation layer occurs when the energy eV_e at which holes are injected into the quantum well is equal to the energy, $\epsilon(\mathbf{k}_{\parallel})$, of a quasibound state of the quantum well. In the absence of scattering, resonant tunneling can only occur with the conservation of energy and in-plane wave vector $\mathbf{k}_{\parallel}=(k_x,k_y)$. In the presence of an in-plane magnetic field B applied along the x axis, the tunneling holes acquire an additional in-plane wave-vector component along the y axis, $\Delta k_{\parallel}=eB\Delta s/\hbar$, where Δs is the average spatial separation between hole states in the emitter accumulation layer and in the quantum well.[16] This additional wave-vector component is perpendicular to both the current and magnetic field. Since the holes in the emitter accumulation layer form a degenerate gas they tunnel with a range of k vector deter-

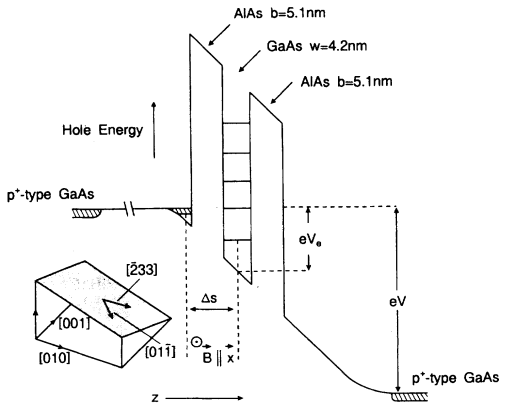

FIG. 1. Band diagram and composition of a p-type resonant tunneling device under an applied voltage V. Holes are injected into the well with an energy eV_e. Inset: position of the (311) plane within the conventional unit cell.

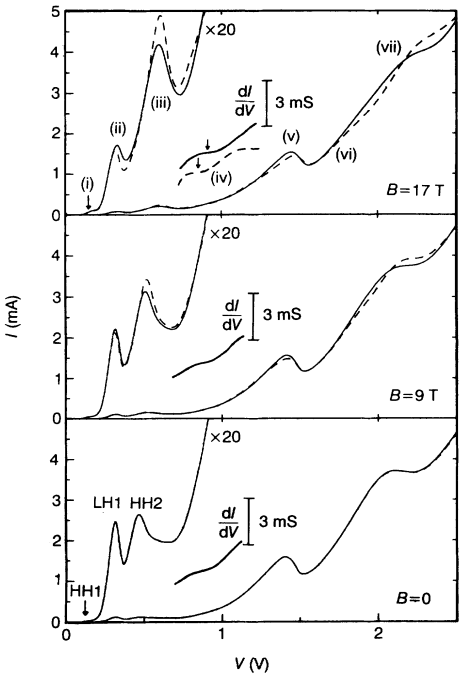

FIG. 2. Current-voltage characteristics at 4.2 K of a p-type resonant tunneling device [grown on a (311)A substrate] at various values of in-plane magnetic field B. Solid curves are for $\mathbf{B}\|[01\bar{1}]$, broken curves are for $\mathbf{B}\|[2\bar{3}\,\bar{3}]$. The effects of anisotropy can be seen clearly, even at $B=9$ T. The position of the weak resonance corresponding to subband iv is indicated in the dI/dV plots as arrows in the $B=17$ T plot.

mined by the accumulation sheet density. This spread tends to broaden the resonances. However, if we neglect the variation of the transmission coefficient with k_y, the resonant peak occurs when there is the largest number of occupied emitter states from which to tunnel. This corresponds to $k_y=k_z=0$ in the emitter accumulation layer.[11,22] The voltage positions V_p of the resonant peaks in the current-voltage characteristics, $I(V)$, are measured as a function of both the direction and magnitude of $\mathbf{B}$. Hence the in-plane energy dispersion of the confined quantum well states can be mapped out.

Figure 2 shows the $I(V)$ characteristics at 4.2 K of the device at various values of in-plane magnetic field. The seven resonant features, each corresponding to resonant tunneling into a quasibound state of the quantum well, are labeled i–vii on the 17-T curves. Unlike the case for a (100) quantum well, the states have an admixed light-hole–heavy-hole character, even at $k_\parallel=0$. Solid curves are for $\mathbf{B}\|[01\bar{1}]$, that is $\mathbf{k}_\parallel$ along $[\bar{2}33]$; broken curves are for $\mathbf{B}\|[2\bar{3}\,\bar{3}]$, that is, $\mathbf{k}_\parallel$ along $[01\bar{1}]$. Two of the quantum-well subbands, iv and vi, produce very weak resonances, which only become visible directly in $I(V)$ at higher magnetic fields; they are clear features in the conductance, dI/dV. We attribute the weakness of these resonances to the camel's-back shape of the $\epsilon(\mathbf{k}_\parallel)$ surfaces of the related quantum-well subbands, as discussed below. The other five resonances are much stronger. Peaks i and ii have a very weak B independence indicating a small $\epsilon(\mathbf{k}_\parallel)$ dispersion. Similar weak dispersion is also found for the two lowest energy subbands in the (100) quantum well.[13,14,16] Some of the peaks show a stronger subband anisotropy. For example, as B is increased from 0 to 17 T, resonance vii moves rapidly to higher voltages, by more than 150 mV, for $\mathbf{B}\|[2\bar{3}\,\bar{3}]$, whereas for $\mathbf{B}\|[01\bar{1}]$ the up-shift is only 90 mV. Subband iv also shows a strong subband anisotropy. However, due to the weakness of this resonance, the effect is only observable in dI/dV. Similar remarks apply to subband vi, which has an even weaker resonance.

We have measured the $I(V)$ characteristics at regular intervals of $\Delta\theta=22.5°$ in the (311) plane and in 1-T steps up to 17 T, corresponding to a maximum in-plane wave vector $\Delta k_\parallel=1.0\pi\times10^6$ cm.$^{-1}$ In this way, following Gennser *et al.*,[18] we can construct $V_p(k_\parallel,\theta)$ contour plots of the dispersion curves for each of the valence-band quantum-well subbands. Figures 3(a), 3(b), and 3(c) show the contour plots of subbands i, iv, and v as examples. The horizontal axis corresponds to the $[01\bar{1}]$ direction. The regions outside the white circles are an extrapolation beyond the range of the measurements. The subbands can be classified into two groups. The first, which includes subbands, i, iii, v, and vii, have the $\epsilon(\mathbf{k}_\parallel)$ surfaces in the form of paraboloids. The constant energy contours are in the form of ellipses with the minimum of hole energy in the subband occurring at $k_\parallel=0$. The anisotropy is small for subbands i and iii. The second type, corresponding to subbands ii, iv, and vi, exhibits the biaxial symmetry of the (311) plane with a camel's-back structure centered at $k_\parallel=0$ in which two minima of the hole energy occur along the $[01\bar{1}]$ axis in the $k_\parallel$ plane. It can be seen that subband i is weakly dispersed and isotropic for $k<1\times10^6$ cm^{-1}, similar in form to the lowest heavy-hole subband of a (100) quantum well.[14] This result is of interest as an anisotropy of the Hall mobility has been observed for the two-dimensional hole gas in the very high mobility p-type heterostructures grown on (311)A.[7] These low-density (4×10^{11} cm^{-2}) heterostructures have a Fermi wave vector $k_F=1.2\times10^6$ cm.$^{-1}$ Our results indicate that this mobility anisotropy is probably due to growth-related corrugations[23] along $[\bar{2}33]$ rather

than a band-structure effect. Figure 3(b) shows the pronounced camel's-back structure of subband iv with minima in hole energy along $[01\bar{1}]$ at $k_{\parallel} \simeq \pm\pi \times 10^6$ cm^{-1}. Thus, for the range of $k_{\parallel}$ achievable with our maximum available magnetic field, this subband has electronlike character for $\mathbf{k}_{\parallel}$ along $[01\bar{1}]$ and hole character for $\mathbf{k}_{\parallel}$ along $[\bar{2}33]$. This type of subband structure with a saddle point at $k_{\parallel}=0$ is not found for unstrained (100) GaAs quantum wells.[10–12]

To compare our observations with theory we have calculated the subbands of an isolated (311) AlAs/GaAs/AlAs valence-band quantum well of width 6 nm on a (311) plane in the absence of applied electric and magnetic fields.[24] The envelope function calculations[10,11] use the six-band Luttinger-Kohn Hamiltonian,[15] which includes the heavy-hole, light-hole, and spin-orbit split-off bands. The Luttinger parameters are quoted in Ref. 16. The results of this calculation for subbands i, iv, and v are shown in Figs. 3(d), 3(e), and 3(f). For all seven subbands, there is qualitative agreement between the general forms of the observed and calculated dispersions. In particular, the resonant magnetotunneling experiment distinguishes correctly between the subbands which have camel's-back and paraboloid energy band structure. The anisotropy of subband i is only evident in the calculated dispersion curves at large $k_{\parallel}$, beyond the range achiev-

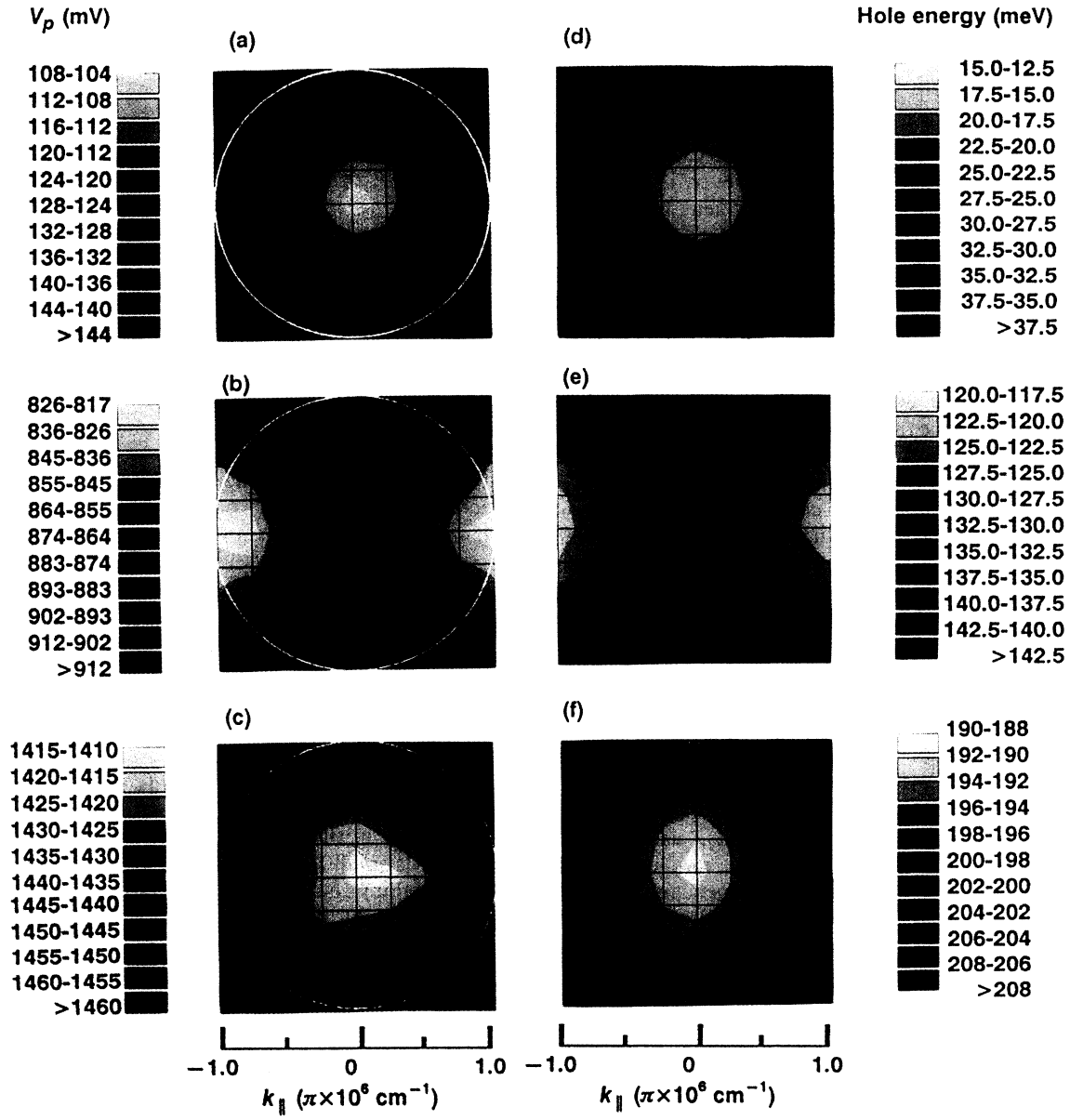

FIG. 3. (a)–(c): Experimental dispersion curves, $V_p(k_{\parallel},\theta)$, for resonances i, iv, and v observed in $I(V)$. The values of $k_{\parallel}$ are obtained from the equation in the text. The regions in the corners beyond the white circle are an extrapolation beyond the range of the measurements. (d)–(f): Contour maps showing the $\epsilon(\mathbf{k}_{\parallel})$ dispersion for the three corresponding quantum-well subbands, calculated in zero electric and magnetic fields, using a six-component envelope-function formalism. The vertical axes correspond to $\mathbf{k}_{\parallel}$ along $[\bar{2}33]$, the horizontal axes correspond to $\mathbf{k}_{\parallel}$ along $[01\bar{1}]$.

able with our maximum available field. We noted earlier that resonant tunneling into subbands iv and vi produces only weak resonant features in $I(V)$, as can be seen in Fig. 2. The calculated $\epsilon(\mathbf{k}_\parallel)$ surface of subband vi has a similar camel's-back-shaped dispersion to that of subband iv.[11] We can account qualitatively for the weakness of these two resonances as follows. Holes tunnel into the quantum well from the lowest subband of the emitter accumulation layer, which at low temperatures is occupied up to its quasi-Fermi-energy. This subband has a small dispersion with positive hole effective mass similar to those shown in Fig. 3(a) for the quantum-well ground state. Increasing the applied bias has the effect of sweeping the emitter $\epsilon(\mathbf{k}_\parallel)$ surface through that of the quantum-well subband. Due to the camel's-back-shaped dispersion of the quantum-well subband, and the requirements of energy and wave-vector conservation, the resonance is spread over a wide range of applied bias and corresponds to a broad but weak feature in $I(V)$.

In order to obtain a quantitative comparison between the data and the calculated band structure, it is necessary to know the charge distribution across the device, including that in the quantum well. This would allow us to calculate the ratio V_p/V_e of the total applied voltage at a resonant peak to the voltage drop between the emitter and quantum well. Such a comparison was possible for similar devices grown on (100) substrates since the charge density in the well could be measured by magneto-oscillations in the $\mathbf{J}\|\mathbf{B}$ geometry.[9] We have not observed these oscillations for a (311)A quantum well. From electrostatic considerations we would expect V_p/V_e to vary over the range from 2 to 4 over the bias range investigated (0–3 V). However, basing the values of V_e on the calculated subband dispersion curves, we obtain values of 1.5, 4, and 2.5 for subbands i, iv, and v, respectively. The discrepancy may be due to a number of factors: e.g., different degrees of charge buildup in the well at different resonances; the effect of the applied electric and magnetic fields in modifying the quantum-well states [the magnetic length $(\hbar/eB)^{1/2}\sim 6$ nm at full field which is approximately the well width]; uncertainty in the Luttinger parameters to which the calculated band structure is known to be sensitive.[11,25]

Despite the lack of quantitative agreement, we conclude that resonant magnetotunneling spectroscopy can reveal the complicated energy band dispersion and anisotropy of the states in a (311)A valence-band quantum well, including a markedly anisotropic camel's-back energy band structure of some of the subbands. We find, however, that the ground-state subband is fairly isotropic.

This work was supported by the Science and Engineering Research Council (United Kingdom), Centre National de la Recherche Scientifique (France), and the European Community. E.C.V. acknowledges financial support from Conselho Nacional de Pesquisas (Brazil).

[1]T. Hayakawa, M. Kondo, T. Suyama, K. Takahashi, S. Yamamoto, and T. Hijikata, Jpn. J. Appl. Phys. **26**, L302 (1987).

[2]B. Gil, Y. El Khalifi, H. Mathieu, C. de Paris, J. Massies, G. Neu, F. Fukunaga, and H. Nakashima, Phys. Rev. B **41**, 2845 (1990).

[3]T. Hayakawa, K. Takahashi, M. Kondo, T. Suyama, S. Yamamoto, and T. Hijikata, Phys. Rev. Lett. **60**, 349 (1988).

[4]C. Mailhot and D. L. Smith, Phys. Rev. B **35**, 1242 (1987).

[5]J. B. Xia, Phys. Rev. B **43**, 9856 (1991).

[6]W. I. Wang, E. E. Mendez, Y. Iye, B. Lee, M. H. Kim, and G. E. Sillman, J. Appl. Phys. **60**, 1834 (1986).

[7]A. G. Davies, J. E. F. Frost, D. A. Ritchie, D. C. Peacock, R. Newbury, E. H. Lindfield, M. Pepper, and G. A. C. Jones, J. Cryst. Growth **111**, 318 (1991).

[8]M. B. Santos, Y. W. Suen, M. Shayegan, Y. P. Li, L. W. Engel, and D. C. Tsui, Phys. Rev. Lett. **68**, 1188 (1992).

[9]R. K. Hayden, T. Takamasu, D. K. Maude, E. C. Valadares, L. Eaves, U. Ekenberg, N. Miura, M. Henini, J. C. Portal, G. Hill, and M. A. Pate, Semicond. Sci. Technol. **7B**, 413 (1992).

[10]U. Ekenberg, W. Batty, and E. P. O'Reilly, J. Phys. (Paris) **48**, C5-553 (1987); R. Wessel and M. Altarelli, Phys. Rev. B **40**, 12 457 (1989).

[11]E. C. Valadares, Phys. Rev. B **46**, 3935 (1992).

[12]S. S. Nedorezov, Fiz. Tverd. Tela (Leningrad) **12**, 2269 (1970) [Sov. Phys. Solid State **12**, 1814 (1971)].

[13]D. A. Broido and L. J. Sham, Phys. Rev. B **31**, 888 (1985); M. Altarelli, U. Ekenberg, and A. Fasolino, *ibid.* **32**, 5138 (1985).

[14]T. Ando, J. Phys. Soc. Jpn. **54**, 1528 (1985).

[15]J. M. Luttinger and W. Kohn, Phys. Rev. **97**, 869 (1955).

[16]R. K. Hayden, D. K. Maude, L. Eaves, E. C. Valadares, M. Henini, F. W. Sheard, O. H. Hughes, J. C. Portal, and L. Cury, Phys. Rev. Lett. **66**, 1749 (1991).

[17]O. H. Hughes, M. Henini, E. S. Alves, M. L. Leadbeater, L. Eaves, M. Davies, and M. Heath, J. Vac. Sci. Technol. B **7**, 1041 (1989).

[18]U. Gennser, V. P. Kesan, D. A. Syphers, T. P. Smith III, S. S. Iyer, and E. S. Yang, Phys. Rev. Lett. **67**, 3828 (1991).

[19]S. Y. Lin, A. Zaslavsky, K. Hirakawa, D. C. Tsui, and J. F. Klem, Appl. Phys. Lett. **60**, 601 (1992).

[20]M. Henini, R. K. Hayden, E. C. Valadares, L. Eaves, G. Hill, and M. A. Pate, Semicond. Sci. Technol. **7**, 267 (1992).

[21]R. K. Hayden, L. Eaves, M. Henini, D. K. Maude, J. C. Portal, and G. Hill, Appl. Phys. Lett. **60**, 1474 (1992).

[22]L. Eaves, R. K. Hayden D. K. Maude, M. L. Leadbeater, E. C. Valadares, M. Henini, O. H. Hughes, J. C. Portal, L. Cury, G. Hill, and M. A. Pate, in *High Magnetic Fields in Semiconductor Physics III,* edited by G. Landwehr, Springer Series in Solid State Sciences Vol. 101 (Springer-Verlag, Berlin, 1992); p. 645.

[23]R. Nötzel, L. Däweritz, N. N. Ledentsov, and K. Ploog, Surf. Sci. **267**, 209 (1992).

[24]The dispersion curves of holes in an isolated valence-band quantum well do not differ appreciably from those of a well with finite barriers if the barriers are sufficiently wide, as is the case here. See R. Wessel and M. Altarelli, Phys. Rev. B **39**, 10 246 (1989).

[25]N. Binggeli and A. Baldereschi, Phys. Rev. B **43**, 14 734 (1991).

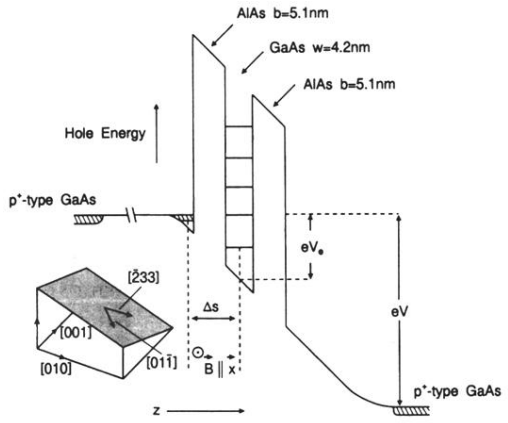

FIG. 1. Band diagram and composition of a p-type resonant tunneling device under an applied voltage V. Holes are injected into the well with an energy eV_e. Inset: position of the (311) plane within the conventional unit cell.

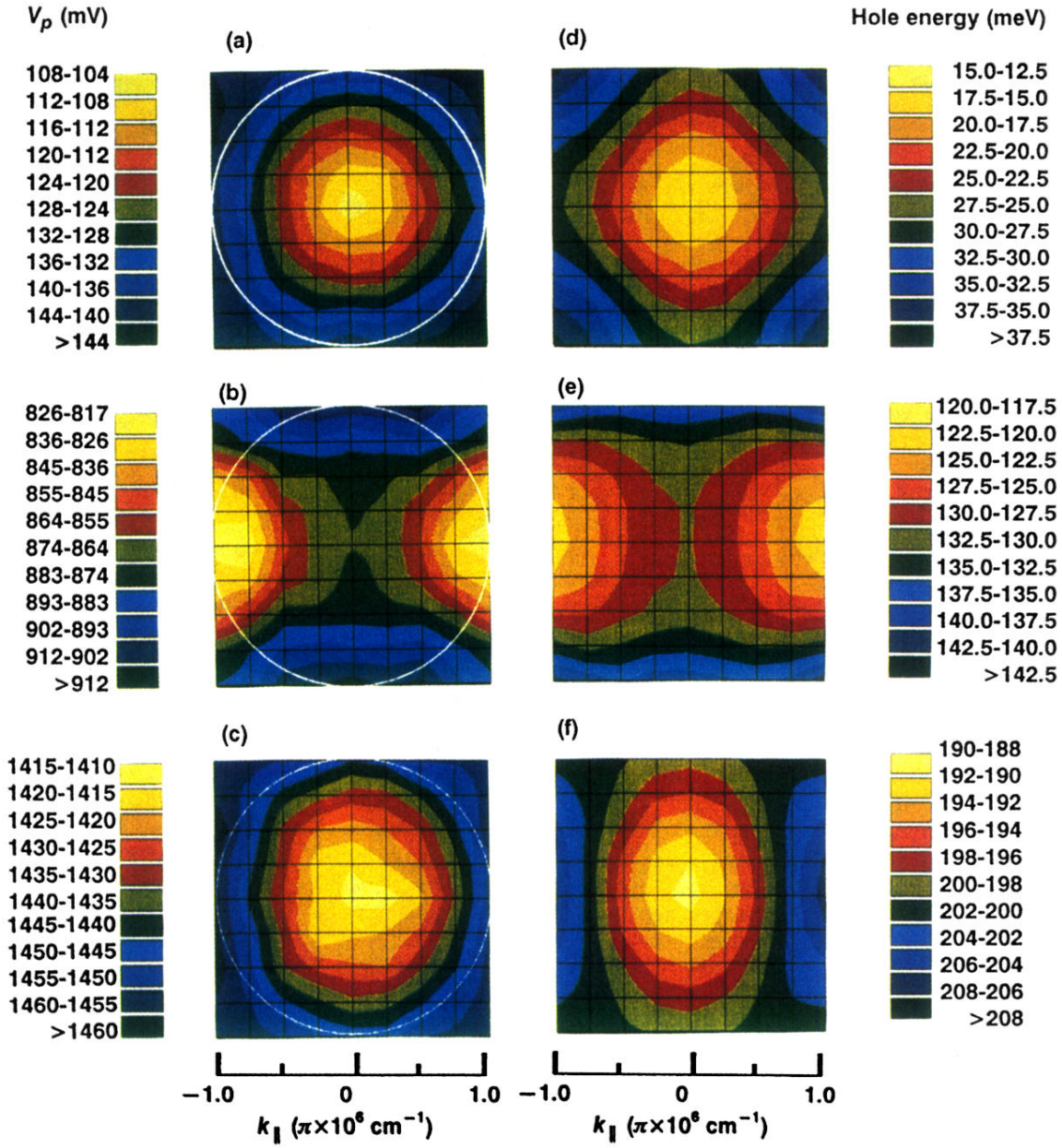

FIG. 3. (a)–(c): Experimental dispersion curves, $V_p(k_\parallel,\theta)$, for resonances i, iv, and v observed in $I(V)$. The values of $k_\parallel$ are obtained from the equation in the text. The regions in the corners beyond the white circle are an extrapolation beyond the range of the measurements. (d)–(f): Contour maps showing the $\epsilon(\mathbf{k}_\parallel)$ dispersion for the three corresponding quantum-well subbands, calculated in zero electric and magnetic fields, using a six-component envelope-function formalism. The vertical axes correspond to $\mathbf{k}_\parallel$ along $[\bar{2}33]$, the horizontal axes correspond to $\mathbf{k}_\parallel$ along $[01\bar{1}]$.